ACS APPLIED MATERIALS & INTERFACES

Research Article

www.acsami.org

Self-Lubricity of WSe_x Nanocomposite Coatings

S. Domínguez-Meister,[†] M. Conte,[‡,§] A. Igartua,[‡] T. C. Rojas,[†] and J. C. Sánchez-López*[,†]

[†]Instituto de Ciencia de Materiales de Sevilla, Avda. Américo Vespucio 49, 41092 Sevilla, Spain

[‡]IK4-Tekniker, Polo Tecnológico de Guipúzcoa, Calle Iñaki Goenaga 5, 20600 Eibar, Spain

ABSTRACT: Transition metal chalcogenides with lamellar structure are known for their use in tribological applications although limited to vacuum due to their easy degradation in the presence of oxygen and/or moisture. Here we present a tailored WSe_x coating with low friction (0.07) and low wear rates (3×10^{-7} mm^3 Nm^{-1}) even in ambient air. To understand the low friction behavior and lower chemical reactivity a tribological study is carried out in a high-vacuum tribometer under variable pressure (atmospheric pressure to 1×10^{-8} mbar). A detailed investigation of the film nanostructure and composition by advanced transmission electron microscopy techniques with nanoscale resolution determined that the topmost layer is formed by nanocrystals of WSe_2 embedded in an amorphous matrix richer in W, a-W(Se). After the friction test, an increased crystalline order and orientation of WSe_2 lamellas along the sliding direction were observed in the interfacial region. On the basis of high angle annular dark field, scanning transmission electron microscopy, and energy dispersive X-ray analysis, the release of W atoms from the interstitial basal planes of the a-W(Se) phase is proposed. These W atoms reaching the surface, play a sacrificial role preventing the lubricant WSe_2 phase from oxidation. The increase of the WSe_2 crystalline order and the buffer effect of W capturing oxygen atoms would explain the enhanced chemical and tribological response of this designed nanocomposite material.

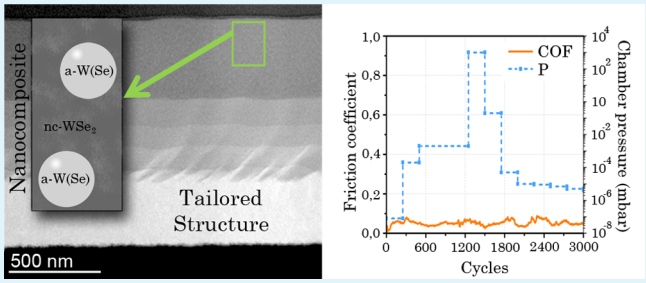

KEYWORDS: *tungsten selenide, Raman, electron microscopy, nanostructure, friction*

1. INTRODUCTION

Smart surface engineering and coating technologies have improved over the years, and now they can be used to meet the increasingly stringent and multifunctional application needs of operational conditions of engine systems, advanced machining, and manufacturing applications.[1−4] Specifically, by designing and using smart tribological coating architectures, researchers have already pioneered the development of a variety of nanocomposite and/or nanostructured coatings providing longer lifetime and enhanced performance under variable working conditions.[5,6] Poor or inefficient lubrication may result in high friction and wear losses, which can, in turn, adversely affect the fuel economy and durability of engines and tools. When used on a lubricated surface, a solid lubricant film may substantially increase the load-bearing capacity and lubricity of that surface by shearing easily. If liquid lubricant fails, solid lubricant can carry the load and prevent direct metal-to-metal contact. Lamellar solid lubricants (such as MoS_2, graphite, hexagonal boron nitride) and soft metals (such as Ag, Au, In, Sn, Pb) in the form of thin films or added to oils and greases in the form of nanoparticles can increase their antifriction and antiwear capabilities.[7−9]

Transition metal (TM) sulfides (MoS_2, WS_2) are well-known for their lubricant properties. The low friction is attributed to their anisotropic layered structure, where the adjacent lamellae with strong covalent bonding interact through relatively weak van der Waals forces. The orientation of the basal planes parallel to the surface in contact provides the easy inter- and intracrystalline slipping. The sliding process induces a preferred orientation in the contacting layer, so that (002)-oriented transfer layer and basally oriented sulfide wear tracks are generated during the steady state.[10] However, their application is limited to vacuum or dry environments because of the sensitivity to humid air.[11] When the S-TM-S planes are oriented perpendicular to the substrate (that is, in the (100) orientation), the exposed edges of these atomic planes are exposed to the atmosphere and oxidized. Improving this tribological performance has been an active area of study particularly for space components that require testing or storage periods on Earth. Increased wear resistance and load-bearing capacity have been reported by alloying with metals (Ti, Au, Pb, Ni, Cr)[12] or nonmetals (N or carbon).[13] As an alternative, nanoscale multilayer (metal/MoS_2,[14] MoS_2/WS_2[15]) or composite films,[17] with mixed hard and soft lubricant phases (MoS_2/WC;[16] WS_2/WC/DLC;[17] TiN/MoS_x;[18] TiCrBN/WSe_x;[19] WS_2/ZnO;[20] TiSiN/WS_2[21]) have also been studied in the past. One of the most studied systems is the transition metal dichalcogenides mixed with carbon by Polcar & Cavaleiro by cosputtering of the metal sulfides or selenides with graphite.[22,23]

Metal selenides are less studied than sulfides although they have also been object of intense study due to their self-lubricant

Received: January 3, 2015
Accepted: February 26, 2015
Published: February 26, 2015

DOI: 10.1021/am508939s
ACS Appl. Mater. Interfaces 2015, 7, 7979−7986

properties,[24−29] applications in photovoltaics,[30] or ultralow thermal conductivity.[31] They have similar layered crystal structure formed by Se−W−Se platelets although with higher axial ratio of lattice parameters, which facilitates relative motion between layers.[32] They exhibit lower average friction coefficients[22] and have demonstrated to be less sensitive to moisture in the environment.[22,24,26] As a metal, W is preferred to Mo, as WO_3 is slightly more protective than MoO_3 and provides lower friction coefficient (0.2−0.3 vs 0.5−0.6, respectively).[33] They show similar drawbacks than their metal sulfides: low hardness, low adhesion to the substrate, and lacking bearing capacity as well as high wear rate and friction coefficient in humid air. The influence of oxygen in the alteration of the friction mechanism is still controversial. The formation of a surface tribolayer by reorientation of the basal planes parallel to the surface would avoid the combination of the oxygen with the dangling bonds.[34]

In previous work, a tailored microstructure of a WSe_x coating was deposited by nonreactive magnetron sputtering with argon using a WSe_2 target, and a time-dependent direct current (d.c.)-pulsed bias. The microstructure was formed by three different sublayers and a variable Se/W ratio along its growing direction (W rich on bottom and Se rich on top). This engineered architecture was responsible for good mechanical properties (H = 5 GPa; E = 90 GPa), low friction (0.07), and low wear rates in ambient air (3×10^{-7} mm^3 Nm^{-1}).[35] In this paper the tribological properties are measured in the high-vacuum tribometer CATRI © IK4-TEKNIKER under variable ambient pressures (atmospheric pressure to 1×10^{-8} mbar). A particular nanostructural study by advanced transmission electron microscopy and analytical tools with nanometric resolution will enable determination of the friction mechanism under variable surrounding atmosphere. The improved performance of this tailored WSe_x lubricant material is highlighted and discussed for tribological applications.

2. EXPERIMENTAL SECTION

Tribological tests were carried out in the CATRI © IK4-TEKNIKER HV tribometer with a 3 mm 100Cr6 ball with variable surrounding atmosphere (atmospheric pressure to 1×10^{-8} mbar). The WSe_x samples deposited onto a silicon substrate were supported in a vertical oscillating rod that moves in the sliding direction. A mechanical action is exerted to the sample by a static pin mounted at the end of a two positioning stage (Y,Z) device. The Z-stage is used to apply the normal load, while the Y-stage is used to perform multiple parallel measurements on the flat sample. Reciprocating tests were done at 1 N of applied load (maximum contact pressure of ∼1 GPa), stroke length of 2 mm, and 2 mm/s of linear speed during 1250 cycles. Long duration tests were performed in a ball-on-disk CSM tribometer using a 6 mm 100Cr6 ball at 5 cm/s of sliding speed and 2 N of applied load during 150 000 and 250 000 cycles.

Raman spectral measurements (200−1800 cm^{-1}) were performed with a LabRAM (Horiba Jobin Yvon) spectrometer equipped with a true confocal microscope, a charge-coupled device detector, and a He−Ne laser (532 nm) working at 2.5 mW to avoid sample damaging. All the samples were analyzed with 100 s exposure times and aperture openings of 100 μm using a 100× magnification.

For the advanced microstructural characterization and elucidation of the friction mechanism, cross-sectional specimens prepared by focused ion beam (FIB) were investigated before and after the friction test using a FEI TECNAI G2 F30 S-Twin high-resolution transmission electron microscope (TEM) with scanning TEM capabilities operating at 300 kV, with 0.2 nm point resolution, equipped with an HAADF detector with 0.16 nm point resolution from Fischione Instruments, and an INCA X-Max 80 silicon drift detector (SDD) for EDX analysis.

3. RESULTS AND DISCUSION

3.1. Tribological Test Results. Previous publications on tungsten diselenides have reported a better moisture resistance and chemical stability than metal sulfides (MoS_2 or WS_2). In our previous work[35] we found an excellent low-friction behavior (below 0.1) either in air (relative humidity (RH) = 30−40%) or dry nitrogen (RH < 7%). To complete the study of the dependence of the tribological properties with the surrounding media, further tests were performed in variable controlled atmosphere inside a high-vacuum (HV) tribometer. Figure 1

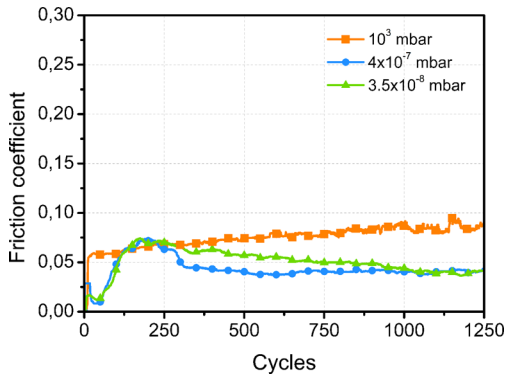

Figure 1. Evolution of the friction coefficient of WSe_x film vs number of sliding cycles for ambient air (1×10^3 mbar), HV-1 (4×10^{-7} mbar), and HV-2 (3.5×10^{-8} mbar). The average friction values obtained for the three conditions are 0.04 ± 0.02 (HV1), 0.05 ± 0.03 (HV2), and 0.08 ± 0.02 (Patm).

displays the friction curves obtained in atmospheric pressure, and two HV values (4×10^{-7} and 3.5×10^{-8} mbar), HV-1 and HV-2, respectively. In dry ambient conditions, the friction coefficient decreases and steadies at ∼0.04, while in air, the value is higher although below 0.1 as commented previously.

Figure 2 reports the evolution of the friction coefficient while changing the atmospheric pressure in a dynamic way, from HV

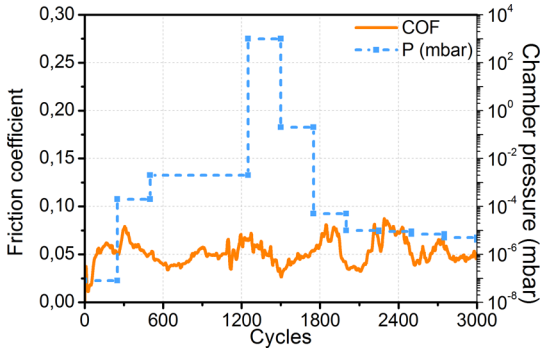

Figure 2. Evolution of the friction coefficient of WSe_x film vs number of sliding cycles at variable pressure in the tribometer chamber.

to atmospheric and then back to HV. It can be observed that the friction coefficient does not alter significantly despite the drastic change of the surrounding media. The average friction coefficient obtained for the entire test is 0.05. The lack of dependence of the tribological response for this type of material represents a significant improvement in respect to diamond-like carbon (DLC) and MoS_2 conventional lubricant solid materials. In these cases, the presence of oxygen or water molecules leads to a degradation of the low-friction conditions and may cause

DOI: 10.1021/am508939s
ACS Appl. Mater. Interfaces 2015, 7, 7979−7986

final failure.[8,36] Although the main use of this layered material as lubricant is under vacuum, this higher chemical stability of the tungsten selenide appears advantageous for situations where the films are exposed to air (during handling or storage) before final application.

According to the friction curves shown in Figure 1 for HV-1 and HV-2, a running-in period is observed for 200−300 cycles where friction rises to a maximum level of 0.07, before a sudden decrease and stabilization around 0.04. These running-in stages are usually associated with removal of surface asperities, native oxide layers, and transfer film buildup. With the aim of dilucidating the influence of ball counterface modification, an interrupted friction test was carried out, stopping at the top of the friction curve. Then, the sample position was changed, and a new test was begun using the same ball to slide onto new fresh surface. The obtained results are shown in Figure 3. The

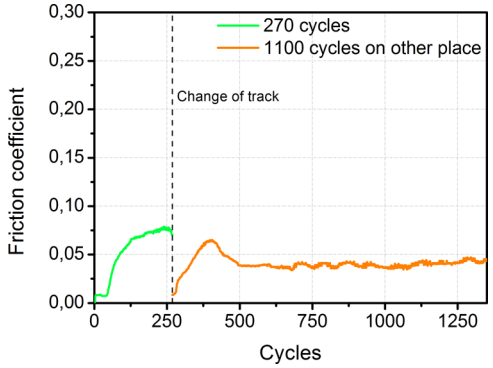

Figure 3. Influence of the surface modification before stabilization of the friction coefficient. The ball rubbed in the first part is lifted and placed on a new fresh surface.

friction coefficient follows exactly the same trend, displaying a transition period before stabilization. This result proves the needs of film surface modification to achieve the ultralow-friction regime.

With the aim of determining the life performance and wear rate of the developed lubricant for the foreseen tribological application, a long duration test was performed in dry nitrogen atmosphere at higher linear speeds in a rotative pin-on-disk using M2 steel substrates. Figure 4 reports the friction evolution until reaching the film failure. This process occurred at ~2×10^5 cycles. Up to this moment very stable and steady-state regime is denoted. Measurement of the film wear track at this point reveals a wear depth of ~450 nm. This value is higher than the thickness of the top lubricant region (I) ranged in 300 nm indicating that the change of tribological behavior is associated with the consumption of the lubricant material. With the aim of establishing the film wear rate a shorter test of 1.5×10^5 cycles was performed. The friction coefficient remained stable and constant, enabling the estimation of the film wear rate. The obtained value was 2×10^{-8} mm^3/Nm, and the wear track depth was found to be ~185 nm confirming that the lubricant layer has not yet worn through.

3.2. Nanostructure and Chemical Composition. To have an insight on the solid lubricant mechanism and their dependency upon the ambient environment, the sample was studied from a structural and compositional point of view using high-resolution transmission electron microscopy (HRTEM), high-angle annular dark field (HAADF), and energy-dispersive X-ray (EDX) spectroscopy working in scanning TEM mode (STEM), before and after the friction test in ambient air. A representative cross-section HAADF-STEM or Z-contrast image of the coating is depicted in Figure 5a where the signal intensity is proportional to $Z^{3/2} \cdot t$ (where Z is the atomic number, and t is the sample thickness). Three main regions with different intensity are observed (labeled as I, II, and III). In the intermediate region (II) a subdivision into three thinner layers is also found. Figure 5b plots the intensity profile of the HAADF signal along the marked line in Figure 5a as well as the atomic percentage of W and Se atoms obtained from the EDX spectra measured using a probe of less than 1 nm. The bottom layer (III) is mainly composed of metallic W, and the Se content is sequentially increasing along the second and third regions to a maximum in the topmost layer. These changes account for the different intensity observed in the HAADF-STEM image (cf. Figure 5a). The average Se/W ratios obtained by integrating the EDX spectra in the different regions are depicted in Figure 5c. This layered structure is a consequence of the modulated pulsed bias applied to the substrate during film growth. Thus, Figure 5d displays the variation of the applied negative voltage going from 55 to 0 V in steps of 11 V/h. Thanks to this sequence a modulation in chemical composition and mechanical properties can be achieved as demonstrated in our previous publication.[35] This tailored architecture is providing the coating with good adhesion to the substrate, film density, mechanical support, and chemical composition for the foreseen tribological application.

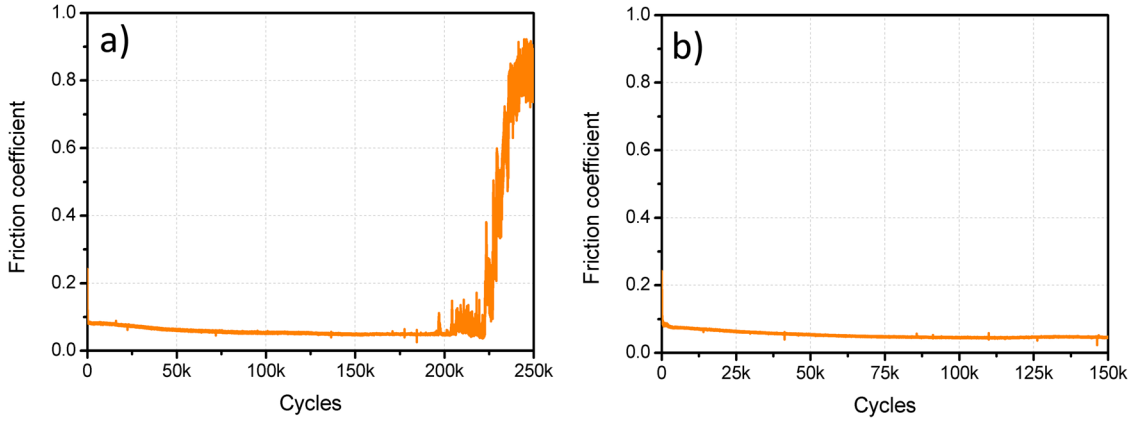

Figure 4. Long duration friction tests performed in dry nitrogen until sudden rise in COF value (a) and just before it (b).

DOI: 10.1021/am508939s
ACS Appl. Mater. Interfaces 2015, 7, 7979−7986

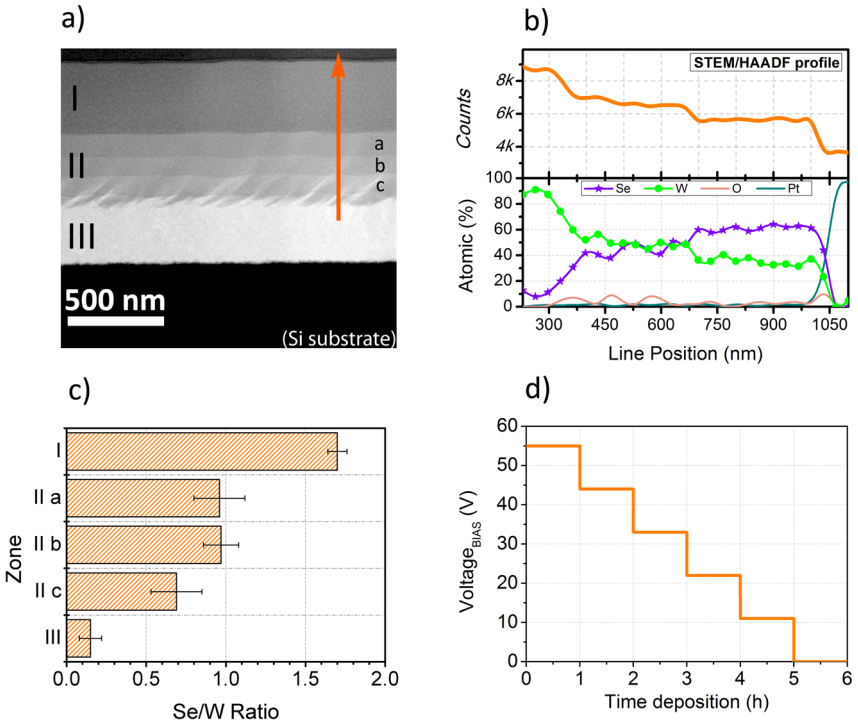

Figure 5. (a) (a) HAADF-STEM cross-section of the WSe_x coating displaying the gradient functional layered architecture. (b) STEM/HAADF signal variation and atomic composition across the profile marked in (a). X-ray used lines for the EDX quantification were Se−L, W−L, O−K, and Pt−L. (d) Variation of the applied negative voltage to the substrates during the growth time in hours.

Figure 6a presents a higher magnification Z-contrast image of the region I measured with higher resolution. Grains with higher intensity of 6−10 nm size are embedded in a matrix of uniform contrast. A detail of this granular structure and the W and Se elemental distribution obtained from the EDX spectra measured along the marked line are depicted in Figure 6b,c. According to the profiles, the W signal rises when crossing the bright grains indicating a higher W content in comparison to the surroundings where the W and Se signals remain comparable. The oxygen signal is very low and does not experience significant changes along the profile. The calculated average Se/W ratios are ranging from 1.0 to 1.3 (inside) to 1.6−1.7 (outside the bright grains). This top layer is responsible for the good tribological behavior as demonstrated in the first part. The friction coefficient remains below 0.1, while this layer is sustaining the contact as demonstrated in the tribological part. The failure of the low-friction regime occurred when entering the second segment (II) where Se/W ≈ 1.

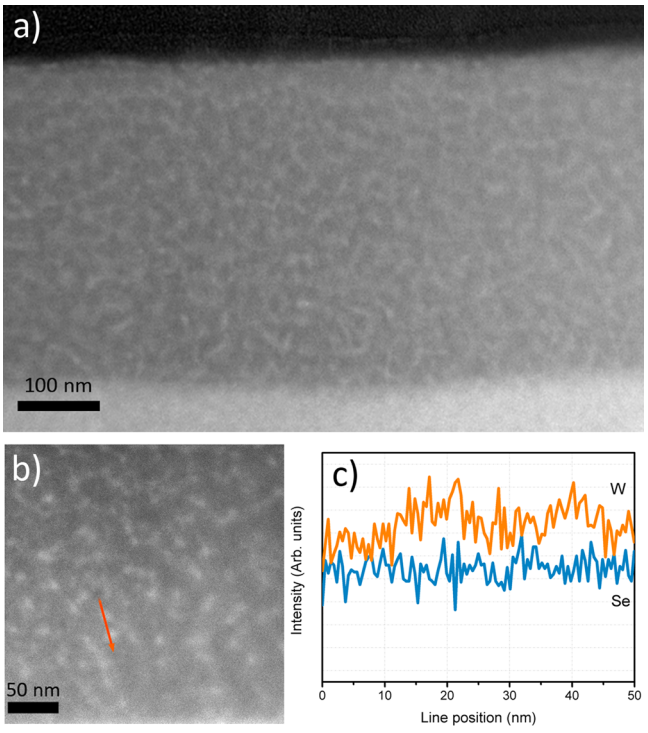

Figure 6. (a) Z-contrast image of the topmost layer. (b) Detail at higher magnification showing two bright grains. (c) Intensity of W and Se signals measured by EDX along the marked profile of Figure 6b.

The HRTEM study of region I shows the presence of lattice fringes, as can be observed in the representative image of Figure 7. A *d*-spacing in the range of 6.7 to 7.6 Å was measured in different micrographs as can be seen in Figure 7a,b. These values are consistent with the distance between two sheets of the lamellar structure (platelet) of the same WSe_2 phase (i.e., (002) spacing). This platelet structure gives rise to the appearance of packs of wires with different orientation that sometimes are curved due to the presence of defect dislocation.[27,37] The size of the ordered WSe_2 domains is ∼3−6 nm, which corresponds to 6−10 platelets. Moreover, lattice fringes of 2.4 and 2.8 (not shown) Å were also measured in different locations of the layer, (cf. Figure 7c) that can be associated with the planes (103) and ($1\bar{1}0$) of the hexagonal WSe_2 phase, respectively. A *d*-spacing of ∼2.2 Å, measured in some small crystals of ∼2 nm size, can be assigned to the family of (110) planes of the body-centered cubic W phase (Figure 7b,c).

As the size of the ordered WSe_2 domains (3−6 nm) is smaller than the size of the W-rich grains (6−10 nm) observed

DOI: 10.1021/am508939s
ACS Appl. Mater. Interfaces 2015, 7, 7979−7986

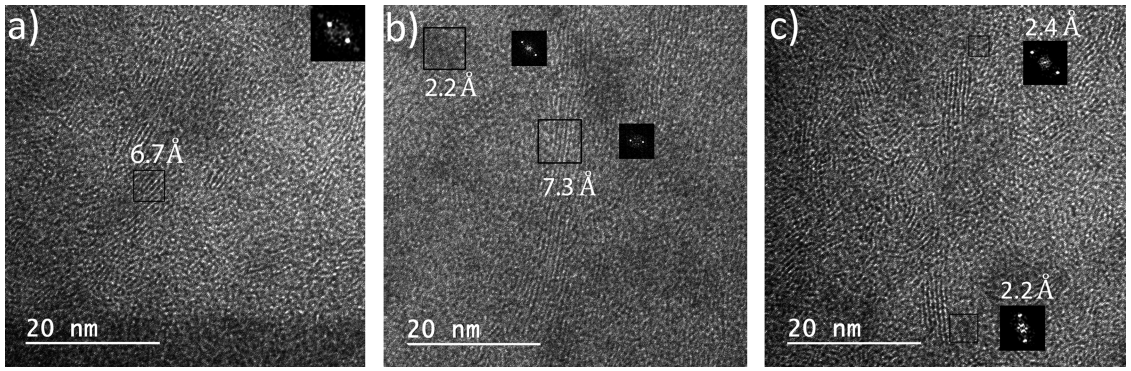

Figure 7. (a–c) HRTEM micrographs showing the different interplanar distances found in the WSe_x samples. The digital diffraction patterns obtained from the marked squares are depicted as insets.

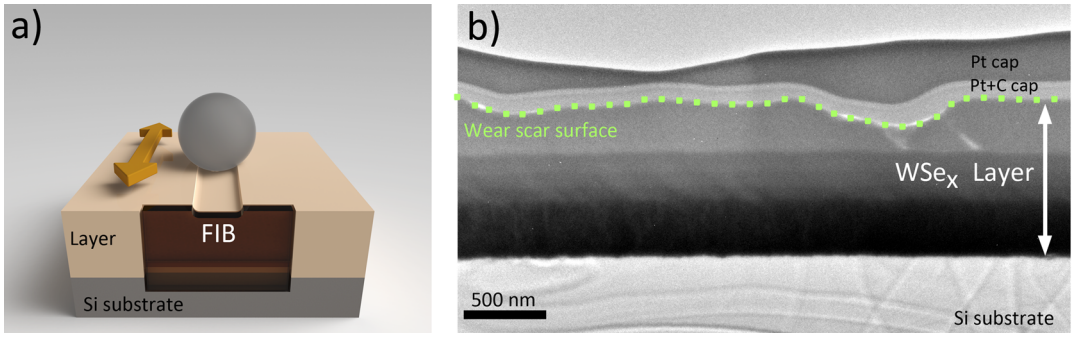

Figure 8. (a) Scheme of the wear track and FIB cross-section; (b) TEM image of the cross-section obtained by FIB.

in the Z-contrast images, one can associate the matte zones in Figure 6a to ordered WSe_2 domains and the brighter ones to the W-rich ones. We should remember that Se/W ratio was less than the stoichiometric value of two in the crystalline domains. While these regions will be referred to as WSe_2, the $WSe_{1.6}$ or $WSe_{1.7}$ should be noted. This Se deficiency is not unusual and has been previously observed in sputtered metal chalcogenides (selenides or sulfides).[19,23,27,28] Likewise, in the regions where W atoms are predominant, Se is present at Se/W ratios of 1.0–1.3, and will be hereafter called W(Se). In the HRTEM images the distances between the ordered WSe_2 domains are ~6–10 nm, similar to the size of W(Se) grains measured in the Z-contrast images. These areas seem to be amorphous suggesting that an excess of W induces an amorphization of the WSe_2 structure. A similar trend has been reported in Ti-WS_2 films[38] when the Ti intercalation between lamellas prevented the crystalline order of the WSe_2 phase. Additionally, the increase and dispersion of the interlamellar distance over the theoretical value for a stoichiometric WSe_2 phase (6.49 Å) support the incorporation of W atoms inside the structure. This increased separation between the basal planes can lead to a friction coefficient reduction by weakening the van der Waals force between the basal planes.[27]

As a result, one can conclude that the sliding contact area is defined as a nanocomposite formed by nonstoichiometric (Se deficient) nanocrystalline WSe_2 surrounded by amorphous W(Se) grains, a-W(Se). Tungsten atoms can be thus intercalated up to certain level between the WSe_2 sheets constituting the ordered WSe_2 fringes detected in the HRTEM pictures. After reaching a certain level of incorporation, additional W atoms may be located outside the crystalline domains forming an amorphous phase WSe_x ($x < 2$) and small nanocrystals of metallic W. The presence of some tungsten oxides in specific points cannot be totally discarded as in certain locations 3–8 atom % of oxygen was measured. W_3O phase has been pointed out as contaminant in a previous publication.[24]

3.3. Friction Mechanism. The contact area of wear track formed after the friction test in air was also chemically and structurally analyzed. A cross-section of the film was prepared in the form of a thin lamella by FIB technique (see Figure 8a). In Figure 8b a representative cross-section TEM image of the WSe_x film in the contact region is shown. A thin protective Pt cap formed by two layers is covering the top surface. The contact interface presents a wavy profile due to the abrasion of surface asperities during the friction process together with some cracks perpendicular to the film surface. Figure 9 shows the comparison of the HAADF-STEM images before and after the friction tests obtained from the interface region. The nanocomposite nanostructure nc-WSe_2/a-W(Se) remains after the test, but a diminution in the density of W(Se) grains in

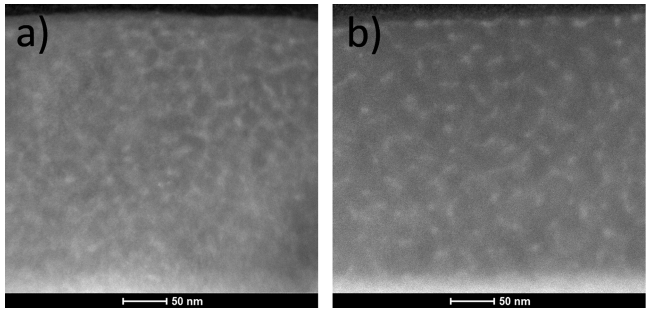

Figure 9. Comparison of the HAADF-STEM images before (a) and after the friction tests (b) obtained from the interface contact region.

DOI: 10.1021/am508939s
ACS Appl. Mater. Interfaces 2015, 7, 7979–7986

general and a certain accumulation of them in the surface in direct contact with the ball are observed.

The HRTEM images obtained for the same contact region (Figure 10) reveal an increase of the order and alignment of the

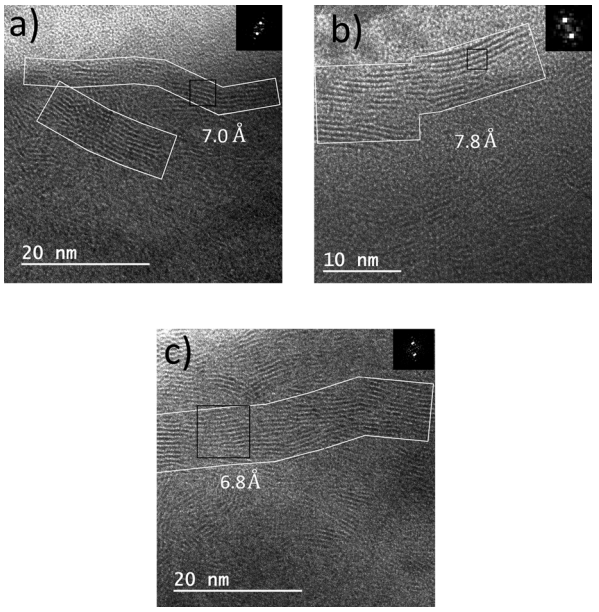

Figure 10. (a, b) HRTEM images obtained from the contact region. An increase ordering and alignment of the basal planes is marked inside the squares. The digital diffraction patterns obtained from the marked squares are depicted as insets.

WSe_2 domains induced by friction. Similar phenomena have been reported in amorphous disordered carbon and metal chalcogenides used as lubricant films.[22,37,39−41] The film structure under pressure and relative motion evolves toward a situation where it minimizes the resistance to shear by alignment of the WSe_2 basal planes parallel to the wear scar surface. The size of the ordered domains grows to 7−14 nm (corresponding to 12−16 platelets), and the measured interlamellar distances ranges between 6.8 and 7.8 Å. The increase of the order and alignment of the WSe_2 regions is simultaneous to the decrease in density of W-rich grains commented on before. This increased crystallinity of the WSe_2 domains is carried out at the expense of a diminution of the a-W(Se) regions. However, in the topmost layer the agglomeration of W atoms can be explained by the consumption of the WSe_2 phase in the lubrication process. The remaining W atoms are thus exposed to air forming tungsten oxides as WO_3 identified by Raman spectroscopy in the debris particles. The presence of this metallic phase, susceptible to be easily oxidized in the contact, helps to preserve the lubricant behavior of the WSe_2 phase and diminish the chemical sensitivity in ambient air.

A further study of the surface modifications induced by friction was done by using Raman confocal spectroscopic analysis on the film wear track. Figure 11a shows the Raman spectrum taken at the end of the long duration test run in dry nitrogen depicted in Figure 4b in comparison to that measured for the initial film. The first observation is the narrowing of the characteristic peak of W−Se bonds at 260 cm^{-1}. The development of the associated bands at 375 and 515 cm^{-1} owing to WSe_2 is also found. This supposes an induced structural arrangement of the WSe_2 structure upon friction in agreement with the HRTEM analysis of the wear track. Figure 11b presents the Raman spectra of the wear tracks as a function of the surrounding environment. This comparison allows concluding an enhanced signal of the above-mentioned peaks in the sequence (atmospheric pressure, HV-1, HV-2). This indicates that in the absence of residual gas the increase of the crystallinity and alignment of the WSe_2 nanocrystals are favored. These results confirm and support the structural arrangements observed by TEM and the decrease of the friction coefficient by easy shear of the basal planes oriented parallel to the wear scar surface.

4. CONCLUSIONS

Surface engineering has enabled the design of a tailored architecture based on W−Se suitable for low-friction and wear properties. This developed material decreases the oxygen and moisture sensitivity as compared to well-known solid lubricants for vacuum and space applications, such as MoS_2. This functional coating is formed by a multiple architecture comprised of a bottom layer rich in W (ensuring a good mechanical support and adhesion strength to the steel substrate), an intermediate segment formed by three sublayers (allowing a gradient transition toward the functional lubricant

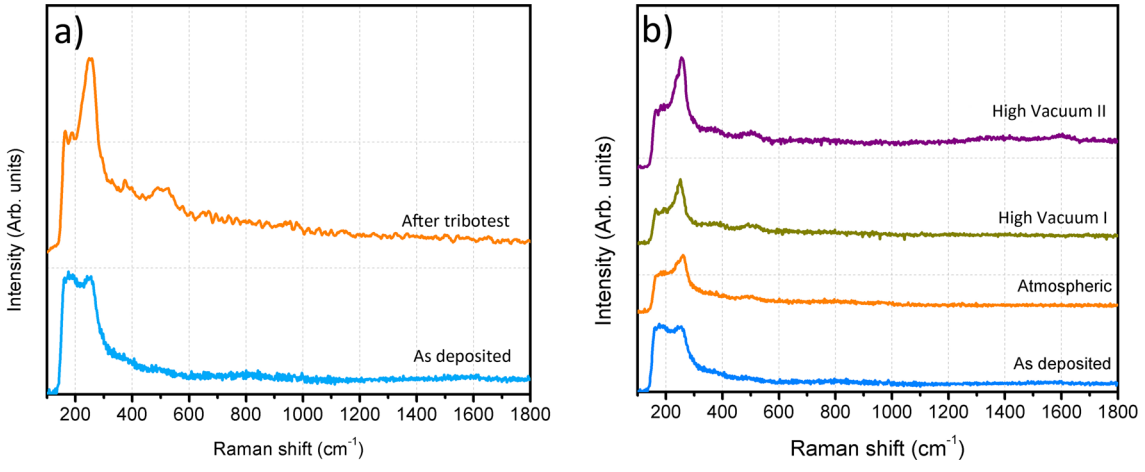

Figure 11. (a) Raman spectra obtained from the wear track after long duration tribological test run in dry nitrogen in comparison with the initial one. (b) Raman spectra measured from the wear track obtained under atmospheric, HV-1, and HV-2 environments.

DOI: 10.1021/am508939s
ACS Appl. Mater. Interfaces 2015, 7, 7979−7986

topmost layer), and a toplayer formed by a nanocomposite structure based on nanocrystals of WSe_2 and amorphous W(Se) phase. The friction coefficient is found to be below 0.1 even in ambient air. The Raman and HRTEM analyses have proven that the tribological stresses are operative hundreds of nanometers below the contact interface although the most relevant changes affect the interfacial layer (5−10 basal planes). Advanced TEM evidenced that the friction process produces an increase of the crystalline domains and alignment of the WSe_2 platelets parallel to the surface. The interstitial W is released from the interlamellar space and diffuses to the surface where it oxidizes in case of ambient air. These sacrificial W atoms help to prevent the oxidation of the WSe_2 phase in ambient conditions supporting the improved performance of this system as a solid lubricant film with less oxygen sensitivity.

AUTHOR INFORMATION

Corresponding Author

*E-mail: jcslopez@icmse.csic.es.

Present Address

[§]Anton Paar TriTec SA, Rue de la Gare 4, 2034 Peseux, Switzerland and Empa, Laboratory for Mechanics of Materials and Nanostructures, Feuerwerkstrasse 39, 3602 Thun, Switzerland.

Notes

The authors declare no competing financial interest.

ACKNOWLEDGMENTS

The Spanish MEC (Project Nos. MAT2010-21597-C02-01; MAT2011-29074-C02-01, and CONSOLIDER FUNCOAT CSD2008-00023), European Union (CT-REGPOT-2011-1-285895 AL-NANOFUNC), and Junta de Andalucía. The FIB lamella preparation has been conducted in the "Laboratorio de Microscopias Avanzadas" at "Instituto de Nanociencia de Aragon - Universidad de Zaragoza". Authors acknowledge the LMA-INA for offering access to their instruments and expertise.

REFERENCES

(1) Holmberg, K.; Matthews, A.; Ronkainen, H. Coatings Tribology−Contact Mechanisms and Surface Design. *Tribol. Int.* **1998**, *31*, 107−120.

(2) Enomoto, T.; Sugihara, T. Improvement of anti-Adhesive Properties of Cutting Tool by nano/micro Textures and its Mechanism. *Procedia Eng.* **2011**, *19*, 100−105.

(3) Veprek, S.; Veprek-Heijman, M. G. J.; Karvankova, P.; Prochazka, J. Different Approaches to Superhard Coatings and Nanocomposites. *Thin Solid Films* **2005**, *476*, 1−29.

(4) Musil, J.; Vlcek, J.; Zeman, P. Hard Amorphous Nanocomposite Coatings with Oxidation Resistance above 1000 °C. *Adv. Appl. Ceram.* **2008**, *107*, 148−154.

(5) Muratore, C.; Voevodin, A. A. Chameleon Coatings: Adaptive Surfaces to Reduce Friction and Wear in Extreme Environments. *Annu. Rev. Mater. Res.* **2009**, *39*, 297−324.

(6) Aouadi, S. M.; Paudel, Y.; Simonson, W. J.; Ge, Q.; Kohli, P.; Muratore, C.; Voevodin, A. A. Tribological Investigation of Adaptive $Mo_2N/MoS_2/Ag$ Coatings with High Sulfur Content. *Surf. Coat. Technol.* **2009**, *203*, 1304−1309.

(7) Abad, M. D.; Sanchez-Lopez, J. C. Tribological Properties of Surface-Modified Pd Nanoparticles for Electrical Contacts. *Wear* **2013**, *297*, 943−951.

(8) Holmberg, K.; Matthews, A. *Coatings Tribology, Tribology, and Interface Engineering Series;* Elsevier: The Netherlands, 2009; Vol. *56*.

(9) Erdemir, A. Review of Engineered Tribological Interfaces for Improved Boundary Lubrication. *Tribol. Int.* **2005**, *38*, 249−256.

(10) Fayeulle, S.; Ehni, P. D.; Singer, I. L. In *Mechanics of Coatings, Tribology Series;* Dowson, D., Ed.; Elsevier: The Netherlands, 1990; Vol. *17*, pp 129−138.

(11) Nabot, J.; Aubert, A.; Gillet, R.; Renaux, P. Cathodic Sputtering for Preparation of Lubrication Films. *Surf. Coat. Technol.* **1990**, *43/44*, 629−639.

(12) Simmonds, M. C.; Savan, A.; Pflüger, E.; Van Swygenhoven, H. Mechanical and Tribological Performance of MoS_2 Co-sputtered Composites. *Surf. Coat. Technol.* **2000**, *126*, 15−24.

(13) Nossa, A.; Cavaleiro, A.; Carvalho, N. J. M.; Kooi, B. J.; De Hosson, J.Th.M. On the Microstructure of Tungsten Disulfide Films Alloyed with Carbon and Nitrogen. *Thin Solid Films* **2005**, *484*, 389−395.

(14) Savan, A.; Pflüger, E.; Goller, R.; Gissler, W. Use of Nanoscaled Multilayer and Compound Films to Realize a Soft Lubrication Phase Within a Hard, Wear-Resistant Matrix. *Surf. Coat. Technol.* **2000**, *126*, 159−165.

(15) Watanabe, S.; Noshiro, J.; Miyake, S. Tribological Characteristics of WS_2/MoS_2 Solid Lubricating Multilayer Films. *Surf. Coat. Technol.* **2004**, *183*, 347−351.

(16) Oñate, J. I.; Brizuela, M.; García-Luis, A.; Braceras, I.; Viviente, J. L. Improved Tribological Behaviour of MoS_2 Thin Solid Films Alloyed with WC. In *9th European Space Mechanisms and Tribology Symposium;* ESA Publications: Noordwijk, Netherlands, 2001; Vol. *480*, pp 257−262.

(17) Voevodin, A. A.; Zabinski, J. S. Supertough Wear-Resistant Coatings with "Chameleon" Surface Adaptation. *Thin Solid Films* **2000**, *370*, 223−231.

(18) Gangopadhyay, S.; Acharya, R.; Chattopadhyay, A. K.; Paul, S. Composition and Structure-Property Relationship of Low Friction, Wear Resistant TiN-MoS_x Composite Coating Deposited by Pulsed Closed-Field Unbalanced Magnetron Sputtering. *Surf. Coat. Technol.* **2009**, *203*, 1565−1572.

(19) Shtansky, D. V.; Sheveyko, A. N.; Sorokin, D. I.; Lev, L. C.; Mavrin, B. N.; Kiryukhantsev-Korneev, Ph.V. Structure and Properties of Multi-Component and Multilayer TiCrBN/WSe_x Coatings Deposited by Sputtering of TiCrB and WSe_2 Targets. *Surf. Coat. Technol.* **2008**, *202*, 5953−5961.

(20) Prasad, S. V.; McDevitt, N. T.; Zabinski, J. S. Tribology of Tungsten Disulfide-Nanocrystalline Zinc Oxide Adaptive Lubricant Films from Ambient to 500 °C. *Wear* **2000**, *237*, 186−196.

(21) Li, S.; Deng, J.; Yan, G.; Zhang, K.; Zhang, G. Microstructure, Mechanical Properties and Tribological Performance of TiSiN-WS_2 Hard-Lubricant Coatings. *Appl. Surf. Sci.* **2014**, *309*, 209−217.

(22) Polcar, T.; Cavaleiro, A. Review on Self-Lubricant Transition Metal Dichalcogenide Nanocomposite Coatings Alloyed with Carbon. *Surf. Coat. Technol.* **2011**, *206*, 686−695.

(23) Evaristo, M.; Polcar, T.; Cavaleiro, A. Can W-Se-C Coatings Be Competitive to W-S-C Ones? *Plasma Processes Polym.* **2009**, *6*, S92−S95.

(24) Shtansky, D. V.; Lobova, T. B.; Fominski, V.Yu.; Kulinich, S. A.; Lyasotsky, I. V.; Petrzhik, M. I.; Levashov, E. A.; Moore, J. J. Structure and Tribological Properties of WSe_x, WSe_x/TiN, WSe_x/TiCN and WSe_x/TiSiN Coatings. *Surf. Coat. Technol.* **2004**, *183*, 328−336.

(25) Fominski, V.Yu.; Nevolin, V. N.; Romanov, R. I.; Titov, V. I.; Scharff, W. Tribological Properties of Pulsed Laser Deposited WSe_x(Ni)/DLC Coatings. *Tribol. Lett.* **2004**, *17*, 289−394.

(26) Kubart, T.; Polcar, T.; Kopecky, L.; Novak, R.; Novakova, D. Temperature Dependence of Tribological Properties of MoS_2 and $MoSe_2$ Coatings. *Surf. Coat. Technol.* **2005**, *193*, 230−233.

(27) Hu, J. J.; Zabinski, J. S.; Bultman, J. E.; Sanders, J. H.; Voevodin, A. A. Structure Characterization of Pulsed Laser Deposited MoS_x-WSe_y Composite Films of Tribological Interests. *Tribol. Lett.* **2006**, *24*, 127−135.

(28) Fominski, V.Yu.; Gregoriev, S. N.; Celis, J. P.; Romanov, R. I.; Oshurko, V. B. Structure and Mechanical Properties of W-Se-C/Diamond-Like Carbon and W-Se/Diamond-Like Carbon Bi-Layer Coatings Prepared by Pulsed Laser Deposition. *Thin Solid Films* **2012**, *520*, 6476.

DOI: 10.1021/am508939s
ACS Appl. Mater. Interfaces 2015, 7, 7979−7986

(29) Gregoriev, S. N.; Fominski, V.Yu.; Gnedovets, A. G.; Romanov, R. I. Experimental and Numerical Study of the Chemical Composition of WSe_x Thin Films Obtained by Pulsed Laser Deposition in Vacuum and in a Buffer Gas Atmosphere. *Appl. Surf. Sci.* **2012**, *258*, 7000−7007.
(30) Guettari, N.; Ouerfelli, J.; Bernède, J. C.; Khelil, A.; Pouzet, J.; Conan, A. Photoconductive WSe_2 Thin Films Obtained by Solid State Reaction in the Presence of a Thin Nickel Layer. *Mater. Chem. Phys.* **1998**, *52*, 83−88.
(31) Chiritescu, C.; Cahill, D. G.; Nguyen, N.; Johnson, D.; Bodapati, A.; Keblinski, P.; Zschack, P. Ultralow Thermal Conductivity in Disordered, Layered WSe_2 Crystals. *Science* **2007**, *315*, 351−353.
(32) Jamison, W. E.; Cosgrove, S. L. Friction Characteristics of Transition-Metal Disulfides and Diselenides. *ASLE Trans.* **1970**, *14*, 62−72.
(33) Bhushan, B.; Gupta, B. K. *Handbook of Tribology-Materials, Coatings and Surface Treatments;* McGraw-Hill, Inc.:New York, 1991, 51−66.
(34) Polcar, T.; Evaristo, M.; Stueber, M.; Cavaleiro, A. Mechanical and Tribological Properties of Sputtered Mo-Se-C Coatings. *Wear* **2009**, *266*, 393−397.
(35) Dominguez-Meister, S.; Justo, A.; Sanchez-Lopez, J. C. Synthesis and Tribological Properties of WSe_x Films Prepared by Magnetron Sputtering *Mat. Chem. Phys.* **2013**, *142*, 186−194.
(36) Donnet, C.; Le Mogne, T.; Ponsonnet, L.; Belin, M.; Grill, A.; Patel, V.; Jahnes, C. The Respective Role of Oxygen and Water Vapor on the Tribology of Hydrogenated Diamond-Like Carbon Coatings. *Tribol. Lett.* **1998**, *4*, 259−265.
(37) Polcar, T.; Evaristo, M.; Colaco, R.; Sandu, C. S.; Cavaleiro, A. Nanoscale triboactivity: The Response of Mo-Se-C Coatings to Sliding. *Acta Mater.* **2008**, *56*, 5101−5111.
(38) Scharf, T. W.; Rajendran, A.; Banerjee, R.; Sequed, F. Growth, Structure and Friction Behavior of Titanium Doped Tungsten Disulphide (Ti-WS_2) Nanocomposite Thin Films. *Thin Solid Films* **2009**, *517*, 5666−5675.
(39) Sánchez-López, J. C.; Erdemir, A.; Donnet, C.; Rojas, T. C. Friction-Induced Structural Transformations of Diamondlike Carbon Coatings under Various Atmospheres. *Surf. Coat. Technol.* **2003**, *163*−*164*, 444−450.
(40) Hu, J. J.; Wheeler, R.; Zabinski, J. S.; Shade, P. A.; Shiveley, A.; Voevodin, A. A. Transmission Electron Microscopy Analysis of Mo−W−S−Se Film Sliding Contact Obtained by Using Focused Ion Beam Microscope and In Situ Microtribometer. *Tribol. Lett.* **2008**, *32*, 49−57.
(41) Scharf, T. W.; Goeke, R. S.; Kotula, P. G.; Prasad, S. V. Synthesis of Au−MoS2 Nanocomposites: Thermal and Friction-Induced Changes to the Structure. *ACS Appl. Mater. Interfaces* **2013**, *5*, 11762−11767.

DOI: 10.1021/am508939s
ACS Appl. Mater. Interfaces 2015, 7, 7979−7986